Theoretical and experimental analysis of radiative recombination lifetimes in nonpolar InGaN/GaN quantum dots

Saroj Kanta Patra[*,1,2], Tong Wang[3], Tim J. Puchtler[3], Tongtong Zhu[4], Rachel A. Oliver[4], Robert A. Taylor[3], and Stefan Schulz[1]

[1] Tyndall National Institute, University College Cork, Cork, Ireland
[2] Department of Electrical Engineering, University College Cork, Ireland
[3] Department of Physics, University of Oxford, Parks Road, Oxford, OX1 3PU, UK
[4] Department of Materials Science and Metallurgy, University of Cambridge, 27 Charles Babbage Road, Cambridge, CB3 0FS, UK

Received XXXX, revised XXXX, accepted XXXX
Published online XXXX

Key words: InGaN, quantum dots, radiative lifetime, a-plane, $\mathbf{k}\cdot\mathbf{p}$

[*] Corresponding author: e-mail sarojkanta.patra@tyndall.ie

We present here a combined experimental and theoretical analysis of the radiative recombination lifetime in a-plane $(11\bar{2}0)$ InGaN/GaN quantum dots. The structures have been grown by modified droplet epitaxy and time-resolved photoluminescence measurements have been performed to gain insight into the radiative lifetimes of these structures. This analysis is complemented by multi-band $\mathbf{k}\cdot\mathbf{p}$ calculations. To account for excitonic effects, the $\mathbf{k}\cdot\mathbf{p}$ theory is coupled with self-consistent Hartree calculations. Special attention is paid to the impact of the quantum dot size on the results. Our calculations show that the residual built-in fields in these nonpolar structures are compensated by the attractive Coulomb interaction, leading to the situation that the oscillator strength is almost unaffected by changes in the quantum dot size. Furthermore, our theoretical studies reveal that the radiative lifetimes are one order magnitude lower than values for c-plane systems of identical size and shape. Our theoretical findings are consistent with experimental results. Also the calculated lifetimes are comparable in magnitude to the measured values. The majority of the measured dots produce lifetime values of 250 ps to 300 ps, highlighting the potential of these nanostructures for future high speed single-photon emitters.

1 Introduction Over recent years semiconductor quantum dots (QDs) have attracted considerable interest due to their potential for non-classical light emitters, such as single- and entangled-photon sources [1–3]. Thanks to their large band offsets, QDs based on group III-nitrides have been identified as potential candidates for single-photon emission near room temperature [4,5]. For instance, Holmes and co-workers [5] have demonstrated single-photon emission from GaN/AlGaN QDs, grown along the crystallographic c-axis, up to 350 K. These results clearly demonstrate the benefit of using nitride-based devices for future non-classical light emitters. However, in principle, by understanding the inherent properties of nitride-based nanostructures, the potential of these systems can even be exploited further. For example, while commercial single-photon detectors operate in the blue spectral region, GaN/AlGaN QD systems allow for single-photon emission in the ultraviolet spectral range [6]. By using InGaN-based QDs the emission wavelength can be "tuned" into the blue spectral regime [7]. This has already been highlighted and demonstrated by Jarjour *et al.* [8]. However, so far all these approaches rely on nitride-based QDs grown along the wurtzite c-axis. When growing nitride-based heterostructures along this crystallographic

direction, the optical properties of these systems are significantly affected by the presence of very strong electrostatic built-in fields (order of MV/cm) [9]. These fields arise in part from spontaneous and in part from strain-dependent piezoelectric polarization fields [10]. In c-plane heterostructures, the electrostatic built-in field leads to a spatial separation of electron and hole wave functions resulting, for example, in large radiative recombination lifetimes τ of the order of several ns [11, 12]. Consequently, this results in single-photon emission with a low repetition rate. Since these built-in fields originate from the growth along the polar c-axis, significant research efforts have been directed towards the growth of non- and semipolar heterostructures [13–15]. For instance, nonpolar quantum wells (QWs) should ideally be built-in field free, since here the polar c-axis lies within the growth plane [13]. Thus, applying this concept to InGaN/GaN QDs should allow for significantly reduced radiative lifetimes in comparison to their c-plane counterparts. This will in principle result in faster recombination rates and thus high speed single-photon emission. However, in comparison to nonpolar InGaN/GaN QWs, the electronic and optical properties of nonpolar InGaN dots have not been addressed at the same level of detail. Furthermore, from a theoretical perspective, since QDs are three-dimensional objects, one is still left with nanostructure interfaces that are oriented along the c-axis and semipolar directions. Consequently, residual built-in fields will still be present in nonpolar InGaN/GaN QDs. This gives rise to the question how changes in the QD size and shape affect quantities such as the radiative lifetimes in nonpolar InGaN/GaN QDs, given its importance for the repetition rate of single-photon emission from these structures.

To shed light on this question, we present here a combined theoretical and experimental analysis of the radiative recombination lifetime τ of nonpolar InGaN/GaN QDs. On the experimental side, structures grown by modified droplet epitaxy (MDE), have been studied by time-resolved photoluminescence (TRPL), providing insights into the radiative recombination lifetimes. The theoretical analysis of these structures is carried out by means of $\mathbf{k}\cdot\mathbf{p}$-theory combined with self-consistent Hartree calculations, thereby accounting for Coulomb effects. Our experimental studies reveal very short recombination lifetimes, of the order of a few hundred ps, which are one order of magnitude smaller than those in c-plane dots [16, 17]. This finding is consistent with here presented theoretical predictions. Moreover, our theoretical results show that the attractive Coulomb interaction between electron and hole overcomes the residual built-in field present in nonpolar InGaN/GaN QDs, forming the origin of the measured and calculated fast recombination lifetime. Additionally, our calculations reveal that variations in QD size lead only to small variations in τ values of nonpolar InGaN dots. This observation is consistent with the trend observed in the experiment, when studying the radiative lifetime of the dots as a function of the QD emission energy. All our findings highlight the potential benefit of using nonpolar InGaN/GaN QDs for future high speed single photon sources.

The manuscript is organized as follows. Section 2 describes the experimental techniques for growth and optical characterization of the here studied nonpolar InGaN/GaN QDs. In Sec. 3 the theoretical framework to calculate electronic and optical properties of these systems is discussed. Since the theoretical model requires QD geometries and sizes as inputs, we review in Sec. 4 available data on this question and present the here assumed model geometry. Section 5 addresses both the results of our experiments and calculations. We start in Sec. 5.1 with the experiment and turn then to the calculations in Sec. 5.2. In Sec. 6, we compare our theoretical data both with experimental data obtained here and available literature results. Finally we summarize our findings in Sec. 7.

2 Experimental setup In the following we present and describe the experimental setup for the growth and the optical characterization of self-assembled nonpolar a-plane $(11\bar{2}0)$ InGaN/GaN QDs. The samples were grown by MDE, a metal-organic vapor phase epitaxy (MOVPE) method originally developed for the fabrication of c-plane QDs [18], but adapted to the growth of a-plane QDs by Zhu *et al.* [19]. The MOVPE procedure was carried out in a Thomas-Swan 6×2 inch close-coupled showerhead reactor on r-plane sapphire substrates with precursor gases of ammonia, trimethylindium, and trimethylgallium. Using epitaxial layer overgrowth [20, 21], a-plane pseudo-substrates were prepared to decrease the density of threading dislocations in the wing region [19]. An InGaN epilayer was grown at 695°C and 300 Torr, then immediately annealed under the same conditions in N_2 atmosphere. For QD formation, a 10 nm GaN capping layer is grown at the same temperature first, followed by another 10 nm of GaN at 1050°C in H_2 atmosphere.

For the optical characterization, the samples have been placed in an AttoDRY 800 close-cycle cryostat, and cooled to a stable temperature of 5 K. An 80 MHz Ti:Sapphire laser provides pulsed excitation with a duration of ~ 1 ps. The excitation wavelength is chosen to be 800 nm, in order to enhance the relative absorption of the QDs. Our previous investigations have established that under multi-photon excitation, the relative absorption cross-section is higher for nanostructures with higher degrees of quantum confinement [22]. As our QDs were formed on top of fragmented QWs due to the growth routine, the emission from the underlying QWs would be suppressed under two-photon excitation, making the investigation and analysis of the QD emission more efficient and accurate. The laser beam is coupled into a single-mode fibre with an output lens, transmitting the spatially filtered and collimated laser beam to a $100\times$ objective (NIR, 0.5 N.A.). In doing so the beam is focused to a ~ 1 μm spot for the excitation of the sample. The PL is collected by the same objective, directed to a

Shamrock 500i half-metre spectrograph with a 100 μm slit and 1200 l/mm grating, and imaged onto a Peltier-cooled Andor iDus 420 charge-coupled device. Attocube positioners are used to control the precise position of the laser spot on the sample which was cooled in a closed cycle AttoDRY 800 cryostat. When the emission spectrum of a QD is observed, the filtered QD PL is then directed to a photomultiplier tube (PMT) for time-correlated single-photon counting (TCSPC).

3 Theoretical framework In this work we are particularly interested in the analysis of the radiative lifetime τ of nonpolar InGaN/GaN QDs and how this quantity compares to c-plane systems. On the theory side, special attention is paid to the impact of the QD size on the results. In general τ can be calculated from [23]

$$\tau = \frac{2\pi\epsilon_0 m_0 c^3 \hbar^2}{n e^2 (E^{\mathrm{X}})^2 f} \ , \tag{1}$$

where ϵ_0,m_0,c,$\hbar$ denote the vacuum permittivity, the free electron mass, the vacuum speed of light and Planck's constant (divided by 2π). Furthermore, to evaluate Eq. (1), information about the excitonic recombination energy E^{X}, the oscillator strength f and the refractive index n of the matrix material is required. To determine n we apply a Sellimeier type law [24,25], allowing us to calculate n as a function of the wavelength λ via $n(\lambda) = \sqrt{a_n + b_n\lambda^2/(\lambda^2 - c_n^2)}$ with $a_n = 5.15\,\mathrm{nm}$, $b_n = 0.35\,\mathrm{nm}$ and $c_n = 339.8\,\mathrm{nm}$. Here, λ is calculated from E^{X} using the relation $\lambda = hc/E^{\mathrm{X}}$, where h is Planck's constant.

To evaluate the oscillator strength f and the excitonic recombination energy E^{X} one needs to gain insight into the electronic structure of the nanostructure. To this end we apply a flexible $\mathbf{k}\cdot\mathbf{p}$ model, consisting of a single-band effective mass approximation for the electrons and a six band Hamiltonian to describe the valence band states, thus accounting for valence band mixing effects. The model has been implemented in the plane wave based software library S/Phi/nX [26,27]. A discussion of the impact of the different input parameter sets on the electronic and optical properties of InGaN/GaN QDs as a function of the growth plane is given in Ref. [28]. However, it is important to note that there is still a large degree of uncertainty in several key material parameters such as piezoelectric coefficients, band offsets, deformation potentials and especially how these parameters change with composition [10,29–32]. Even though most material parameter sets predict similar trends for polar and non-polar growth planes, absolute numbers might depend on the accurate knowledge of the material parameters and could therefore vary between different sets [33]. The material parameters used in this study are summarized in Table 1.

The $\mathbf{k}\cdot\mathbf{p}$ model allows us now to evaluate the QD single-particle states. To account for excitonic effects, the $\mathbf{k}\cdot\mathbf{p}$ wave functions serve as input for self-consistent Hartree calculations. In doing so, we are left with the following set of equations which have to be solved self-consistently [39]:

$$[H + V_{\mathrm{e}}]\psi_{\mathrm{h}} = E_{\mathrm{h}}^{\mathrm{X}}\psi_{\mathrm{h}} \ , \tag{2}$$

$$[H + V_{\mathrm{h}}]\psi_{\mathrm{e}} = E_{\mathrm{e}}^{\mathrm{X}}\psi_{\mathrm{e}} \ . \tag{3}$$

Here H is the single-particle (empty dot) $\mathbf{k}\cdot\mathbf{p}$ Hamiltonian and the potentials arising from the presence of electron and hole in the dot are denoted by V_{e} and V_{h}, respectively. These contributions can, in general, be calculated via

$$-e|\psi_{\mathrm{e}}|^2 = \epsilon_0\epsilon_r\nabla^2 V_{\mathrm{e}} \ ; \ e|\psi_{\mathrm{h}}|^2 = \epsilon_0\epsilon_r\nabla^2 V_{\mathrm{h}} \, . \tag{4}$$

The exciton recombination energy E^{X} required in Eq. (1) is obtained from [40]

$$E^{\mathrm{X}} = E_{\mathrm{e}}^{\mathrm{X}} - E_{\mathrm{h}}^{\mathrm{X}} - J_{\mathrm{eh}} \ , \tag{5}$$

Table 1 Material parameters used in this study for GaN and InN.

Parameter	GaN	InN
$a_{\mathrm{lat}}(\mathring{A})$ [34]	3.189	3.545
$c_{\mathrm{lat}}(\mathring{A})$ [34]	5.185	5.703
C_{11} (GPa) [35]	368.6	233.8
C_{12} (GPa) [35]	131.6	110.0
C_{13} (GPa) [35]	95.7	91.6
C_{33} (GPa) [35]	406.2	238.3
C_{44} (GPa) [35]	101.7	55.4
$e_{15}(C/m^2)$ [36]	-0.32	-0.42
$e_{31}(C/m^2)$ [36]	-0.44	-0.58
$e_{33}(C/m^2)$ [36]	0.74	1.07
$P_{\mathrm{sp}}(C/m^2)$ [36]	-0.040	-0.049
ε_r [10]	9.6	15.3
E_g (eV) [37]	3.51	0.69
Δ_{CF} (eV) [38]	0.019	0.024
Δ_{SO} (eV) [34]	0.017	0.005
$m_e(m_0)$ [30]	0.209	0.068
$A_1(\hbar^2/2m_0)$ [30]	-5.947	-15.803
$A_2(\hbar^2/2m_0)$ [30]	-0.528	-0.497
$A_3(\hbar^2/2m_0)$ [30]	5.414	15.251
$A_4(\hbar^2/2m_0)$ [30]	-2.512	-7.151
$A_5(\hbar^2/2m_0)$ [30]	-2.510	-7.060
$A_6(\hbar^2/2m_0)$ [30]	-3.202	-10.078
a_c (eV) [34]	-4.08	-7.2
$a_c - D_1$ (eV) [38]	-5.81	-3.64
$a_c - D_2$ (eV) [38]	-8.92	-4.58
D_3 (eV) [38]	5.45	2.68
D_4 (eV) [38]	-2.97	-1.78
D_5 (eV) [38]	-2.87	-2.07
D_6 (eV) [38]	-3.95	-3.02
$E_{P\parallel}$ (eV) [41,30]	18.7	8.742
$E_{P\perp}$ (eV) [41,30]	17.7	8.809
$\Delta E_{\mathrm{VB}}^{\mathrm{InN/GaN}}$ (eV) [31]	0.62	

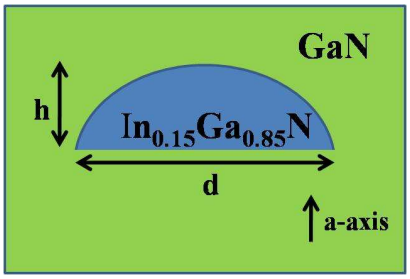

Figure 1 Schematic illustration of the here used lens-shaped $In_{0.15}Ga_{0.85}N$/GaN a-plane dot geometry. The dot diameter is denoted by d and the height by h.

where $E_{\rm h}^{\rm X}$ and $E_{\rm e}^{\rm X}$ are derived from Eqs. (2) and (3). To account for the double counting of the attractive Coulomb interaction in Eqs. (2) and (3), we correct the recombination energy $E^{\rm X}$ by [40]

$$J_{\rm eh} = -e^2 \int\int \frac{|\psi_{\rm e}(\mathbf{r})|^2 |\psi_{\rm h}(\mathbf{r}')|^2}{4\pi\epsilon_r\epsilon_0|\mathbf{r}-\mathbf{r}'|} d^3r d^3r' \, .$$

Equipped with the knowledge about $E^{\rm X}$ and the ground state electron $\psi_{\rm e}$ and hole $\psi_{\rm h}$ wavefunctions, the oscillator strength f is calculated via [23]

$$f = \frac{2\hbar^2}{m_0 E^{\rm X}} \sum_{\alpha} \left| \int \psi_{\rm e}^*(\mathbf{r})(\mathbf{e}\cdot\mathbf{k})\psi_{\rm h}^{\alpha}(\mathbf{r}) d^3r \right|^2 . \quad (6)$$

Here, $\mathbf{e}$ is the light polarization vector of the incident light and $\mathbf{k} = -\mathbf{i}\nabla$. α denotes hole wavefunctions representing the same degenerate hole energy level $E_{\rm h}^{\rm X}$. Making use of the fact that electron and hole wavefunctions can be cast as linear combinations of the product of Bloch functions $|u_i\rangle$ and envelope functions $|\phi_i\rangle$, $\psi = \sum_i |u_i\rangle|\phi_i\rangle$, the integral can be expressed in terms of the Kane matrix element E_p and is proportional to $\langle s|k_i|p_j\rangle = \delta_{i,j}\sqrt{\frac{m_0 E_P}{2\hbar^2}}$. In the following we have used $E_P = (2E_{P\|} + E_{P\perp})/3$ [11], and the values for $E_{P\|}$ and $E_{P\perp}$ have been taken from Refs. [41, 30]. The light polarization vector $\mathbf{e}$ is always chosen to be perpendicular to the sample surface ($\mathbf{e} = (1,1,0)^T$).

Having established the theoretical framework to calculate τ, the QD geometry and size is required as further input for the model. In the next section we will review available experimental data on this question and discuss the model geometry assumed in the theoretical study.

4 Quantum dot geometry and size From an experimental point of view it presents an extremely challenging task to gain insight into the detailed information about the geometric features of the QD, especially after capping these structures [42]. Atomic force microscopy (AFM) studies of the present uncapped nonpolar QD samples reveal nanostructure heights of the order of 7 ± 3 nm [19]. For nonpolar capped GaN/AlGaN QDs typical base diameters of the order of 20 nm have been reported in the literature [43]. This information gives us a good starting point for the size of the structure but not about the dot geometry. In previous theoretical investigations of nonpolar InGaN/GaN QDs lens-shaped dot geometries have been assumed [44,45].

Making use of the available experimental data and previous theoretical assumptions, we model nonpolar InGaN/GaN dots as lens-shaped objects, schematically illustrated in Fig. 1. Taking into account that the dimensions of the dots will be affected by the capping procedure, and aiming to study the impact of the dot size on the results, we assume in our calculations two different scenarios. First, the diameter d of the nanostructure is varied between 6 nm and 24 nm, while keeping the dot height h constant at 2.5 nm. Second, d is kept fixed at 24 nm and h is now allowed to vary between 2 nm and 5 nm. To investigate how the growth plane affects τ, all geometric QD features are carried over to calculations for c-plane dots. Thus when we compare c- and a-plane InGaN/GaN QDs in our theoretical studies, changes in the calculated quantities arise entirely from the difference in the growth plane and not due to variations in QD geometry. It should be noted that even though we carry over geometries and sizes based on assumptions for nonpolar InGaN dots to describe c-plane systems, these assumptions, especially for the dot size, should give a good first approximation of realistic c-plane QDs [46].

With respect to the indium content we have chosen a value of 15%, which is a reasonable value based on the growth conditions used and the measured compositions of multiple quantum well structures grown under similar conditions. We will discuss the impact of the indium content on the results in more detail when we compare theory and experiment in Sec. 6.

Regarding computational details, all calculations have been performed on a supercell with a dimension of $50 \times 50 \times 30$ nm^3, using periodic boundary conditions. Different step sizes are employed along the growth direction and in the growth plane. Along the growth axis we employ a step size of 0.25 nm, while we use 0.5 nm to discretize the in-plane dimension. This accounts for the fact the that the minimum dot height is only 2 nm while the base diameter is at least 6 nm.

5 Results In this section we discuss the results of our experimental and theoretical studies of a-plane $(11\bar{2}0)$ InGaN/GaN QDs. We start with the results from the TRPL measurements in Sec. 5.1. Subsequently, in Sec. 5.2, we analyze the radiative recombination lifetime τ by means of our theoretical framework and also compare c- and a-plane results.

5.1 Optical characterization The radiative lifetime data of 10 typical a-plane InGaN QDs are shown in Fig. 2 as a function of QD emission energy. As these decay times are very short, and close to the instrument response time (IRF) of the PMT ($\sim$ 130 ps), all data were fitted with a

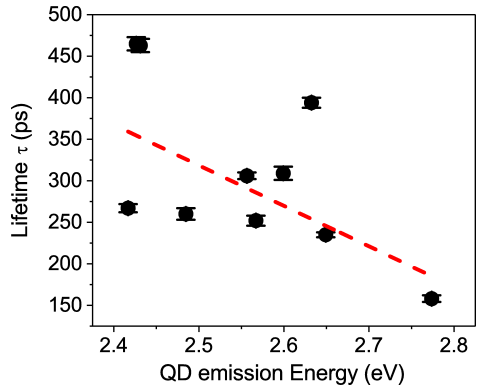

Figure 2 Recombination lifetime τ obtained experimentally as a function of the QD emission energy. The error bars are also indicated in the figure. Also displayed is a linear fit to the experimental data, showing the correlation between lifetime and QD emission energy.

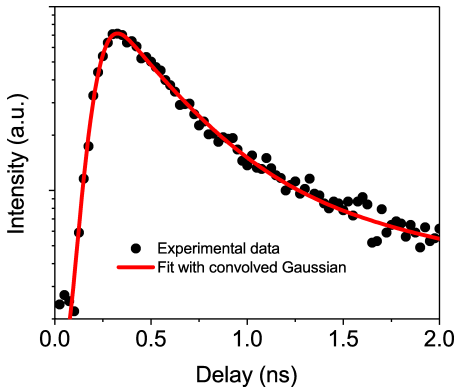

Figure 3 A representative set of experimental TRPL data and the fitting with an exponential decay convolved with a Gaussian function. The extracted radiative lifetime is 306 ps. All data in Fig. 2 were obtained using this method.

modified Gaussian function, where the IRF (assumed to be a Gaussian function) has been convolved with an exponential decay function. The fitted time constant of the exponential was then treated as the exciton radiative lifetime τ. An example of the fitting to experimental TRPL data is shown in Fig. 3, where the use of the convolved function produced a close fit with the results. Based on the method described above, the extracted radiative lifetime from this TRPL plot is 306 ± 4 ps. The fitting with the convolved function hence ensures an accurate lifetime measurement close to the IRF width. In general, lifetimes obtained from our TRPL measurements range from 150 to 500 ps with the majority around 250-300 ps. These values are indeed an order of magnitude smaller than values found in c-plane systems [16, 17]. Our previous studies of nonpolar QDs grown by both MDE and an alternative method show radiative lifetimes [19,47] around 500 ps to 600 ps, consistent with the range of values we report here. Furthermore, we observe here a vague trend that with decreasing QD emission energy the radiative lifetime τ increases. To elucidate this trend, a linear fit to the experimental data is displayed in Fig. 2 showing the correlation between lifetime values and QD emission energy. To achieve a better statistical average, this analysis has to be extended to a much large number of dots. However, this is beyond the scope of the present study. Overall, our experimental data demonstrates that the use of the nonpolar a-plane reduces the undesired quantum confined Stark effect, increasing the exciton oscillator strength and producing much shorter lifetimes, when compared to c-plane systems. It is also noteworthy to mention that the experiment was performed at low temperatures (under 5 K). The measured radiative lifetime only decreases by a small amount at temperatures as high as 200 K (other temperature investigations are beyond the scope of this work). Given that if substantial non-radiative recombination were present it would have a dominant effect at these high temperatures, we conclude that the amount of non-radiative recombination at 5 K, which is likely to be much smaller than that at 200 K, should be close to negligible. In the next section we will address the question of the radiative lifetime from a theoretical perspective.

5.2 Theory Before turning to the comparison between theory and experiment for the radiative lifetimes, we start with an analysis of the oscillator strength f in c- and a-plane dots and how this quantity is affected by changes in the dot size. Having established these general trends in f, we study in a second step how τ changes when the QD size changes.

5.2.1 Analysis of oscillator strength f Here, we study the oscillator strength f as a function of the dot diameter d and the dot height h. We start with d and vary this quantity between 6 nm and 24 nm, while h is kept constant at 2.5 nm. To compare the increase or reduction in f when changing the dot geometry more easily, we work in the following with the *relative* oscillator strength $\tilde{f}^{\beta}(d)$ for c- ($\beta = c$) and a-plane ($\beta = a$) InGaN/GaN QDs. We define this quantity as:

$$\tilde{f}^{\beta}(d) = \frac{f^{\beta}(d)}{f^{\beta}(6)} \ . \tag{7}$$

Here, $f^{\beta}(6)$ denotes the oscillator strength calculated from Eq. (6) for a dot with height $h = 2.5$ nm and a base diameter of $d = 6$ nm. $f^{\beta}(d)$ is the oscillator strength calculated as a function of d. Thus $\tilde{f}^{\beta}(6) = 1$. The results of this analysis are depicted in Fig. 4 with and without Columb interaction for both polar and nonpolar dots. Looking at $\tilde{f}^{\beta}(d)$ without Coulomb effects, we find that in the nonpolar case (open circles), $\tilde{f}^{a}(d)$ decreases by a factor of 2 to a value of $\tilde{f}^{a}(24) = 0.46$ when d changes from 6 nm to 24 nm. A similar behavior is observed for the polar case (open squares), however, here the effect is more pronounced, showing that for $d = 24$ nm $\tilde{f}^{c}(24) \approx 0.30$.

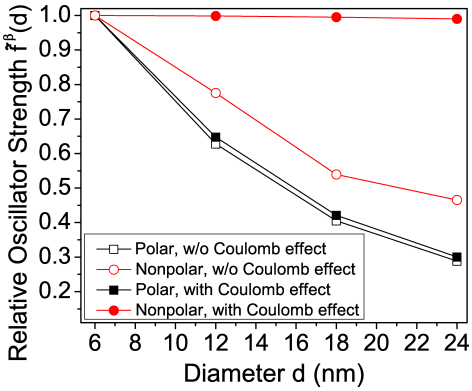

Figure 4 Relative oscillator strength $\tilde{f}^{\beta}(d)$ of polar and nonpolar $In_{0.15}Ga_{0.85}N$/GaN QDs as a function of the base diameter d with and without Coulomb effect. The height h of the dots is kept fixed at 2.5 nm.

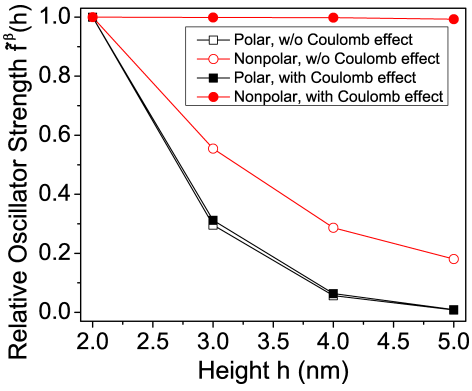

Figure 5 Relative oscillator strength $\tilde{f}^{\beta}(h)$ of polar and nonpolar $In_{0.15}Ga_{0.85}N$/GaN QDs as a function of the dot height h with and without Coulomb effect. The base diameter d of the dots is kept fixed at 24 nm.

This behavior can be explained by the following factors. For both c- and a-plane systems, the increase in d leads to an increase in the QD volume and consequently to an increase in the magnitude of the built-in field [32], which results in a stronger localization of the charge carriers at the interfaces. Therefore, the spatial separation between the carriers is increased, leading to a reduction in $\tilde{f}^{\beta}$. This brings us to another factor that affects f in the nonpolar case. Even though the built-in field is reduced in the a-plane QD, when compared with the c-plane structures, we are left with an increased distance between the two QD interfaces oriented along the c-axis. Consequently, the charge carriers can spatially be separated over a larger distance in the a-plane structure. However, the stronger reduction in $\tilde{f}^{\beta}(d)$ for the c-plane QDs, when compared to the nonpolar structures, is attributed to the fact that the built-in fields are much stronger in the c-plane case. This dominates over the larger spatial extension of the dot along the c-axis in the nonpolar case. Thus, to a first approximation, when neglecting the Coulomb interaction in the system, both a- and c-plane dots show similar trends in terms $\tilde{f}^{\beta}(d)$.

This situation is completely changed when including Coulomb effects in the calculations, as depicted in Fig. 4. Here we find that the attractive Coulomb interaction between electrons and holes overcomes the residual built-in field in the nonpolar case (filled circles), resulting in an almost constant value of $\tilde{f}^{a}(d)$. It is also evident that the Coulomb effect has very little impact on $\tilde{f}^{c}(d)$. Thus the oscillator strength f in the polar case (filled squares) is mainly dominated by the electrostatic built-in field, while the Coulomb effects dominate the wavefunction overlap in the nonpolar case.

To further analyze the impact of the QD size on the results, we have also performed calculations with varying dot heights h. Similar to the above discussions, we define here the relative oscillator $\tilde{f}^{\beta}(h)$, where $\tilde{f}^{\beta}(h)$ is normalized to the oscillator strength of a dot with height $h = 2$ nm. The dot diameter d is kept constant at $d = 24$ nm. Figure 5 shows the variation of $\tilde{f}^{\beta}(h)$ with and without Coulomb effect for both polar and nonpolar InGaN/GaN dots. In comparison to Fig. 4 where we have varied the dot diameter d, we observe here similar trends in $\tilde{f}^{a}(h)$. Again, due to the reduced built-in fields in the a-plane dot when compared to the c-plane structures in the absence of Coulomb effects, $\tilde{f}^{a}(h)$ (open circles) is always larger than $\tilde{f}^{c}(h)$ (open squares). For the largest system studied here, $d = 24$ nm and $h = 5$ nm, $\tilde{f}^{c} \approx 0$ while $\tilde{f}^{a} \approx 0.18$.

When taking Coulomb effects into account, we find again that the oscillator strength $\tilde{f}^{c}$ in the polar structures (filled squares) is dominated by the built-in field, while in the nonpolar system (filled circles) Coulomb effects become important. In the non-polar case, this results in the situation that $\tilde{f}^{a}$ is almost independent of h.

Overall, our analysis reveals that for nonpolar InGaN/GaN QDs variations in the dot size are of secondary importance for the (relative) oscillator strength since the attractive Coulomb effect is dominant. Thus for an accurate theoretical description of the optical properties of these systems, Coulomb effects have to be included. So far we have only studied the relative oscillator strength without directly comparing to experimental measurements of exciton lifetime. We therefore study the radiative recombination lifetime τ and how this quantity changes with variations in the dot geometric features in the next section. The comparison between theory and experiment is addressed in Sec. 6.

5.3 Calculation of radiative lifetime τ Equipped with the knowledge about changes in the oscillator strength f with QD size, the variation of the radiative lifetime τ, Eq. (1), in polar and nonpolar InGaN/GaN dots is studied here. We start our analysis by looking at the impact of the dot diameter d on τ. For this study the height of the

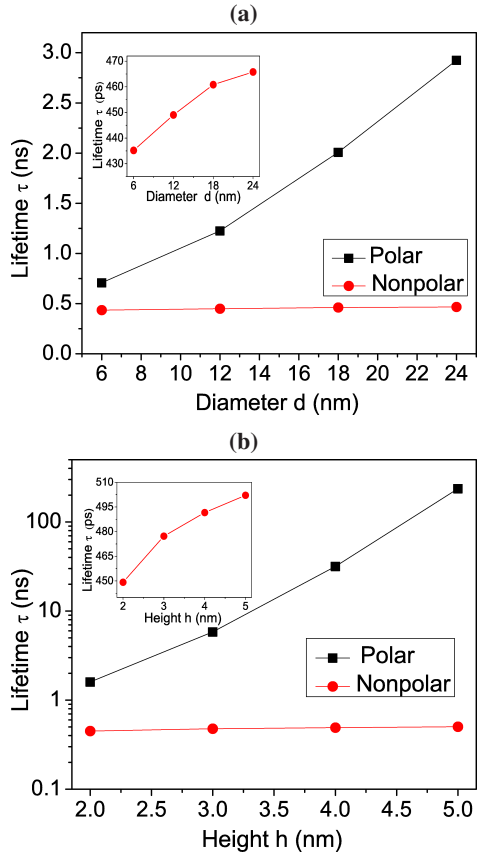

Figure 6 (a) Recombination lifetime τ as a function of QD base diameter d. The dot height is kept fixed at $h = 2.5$ nm (b) Recombination lifetime τ as a function of QD height h. The base diameter of the dot is 24 nm. The inset shows nonpolar data (red circles) separately from the polar data (black squares) to visualize trends more clearly.

dot is chosen to be $h = 2.5$ nm, while the base diameter varies between 6 nm and 24 nm. The calculated lifetimes are displayed in Fig. 6 (a) for the polar (black square) and nonpolar (red circle) InGaN/GaN dots. For the polar QDs we observe that τ increases with increasing dot diameter d. In contrast to this, τ stays approximately constant for the nonpolar system, at least when compared with the polar case. This observation is consistent with the behavior of the oscillator strength discussed in the previous section and displayed in Fig. 4, since τ is inversely proportional to f, cf. Eq. (1). Thus larger values of f lead to smaller values of τ. Looking at the absolute values of τ for both the polar and the nonpolar dots, we find here that for the c-plane dots, values in the range of several nanoseconds are obtained, consistent with literature experimental data [16, 17]. For the nonpolar dots, also displayed in the inset of Fig. 6 (a), our calculated τ values are in the range of 435 ps to 465 ps. It should be noted that this variation, even though $\tilde{f}^a(d)$ is approximately constant, arises from the fact that E^{X} varies when the dot volume increases. In this case, E^{X} is shifted to smaller energies resulting in an increase of τ, given that τ is inversely proportional to E^{X}, cf. Eq. (1).

In the second step, we investigate the impact of the QD height h on τ. In these calculations the dot height ranges from 2 nm to 5 nm. The base diameter for these studies is kept constant at $d = 24$ nm. In the case of the nonpolar dots, the τ values change only slightly from around 450 ps to approximately 500 ps when h changes from 2 nm to 5 nm (see inset of Fig. 6 (b)). This finding is consistent with the observation that the oscillator strength f stays approximately constant when changing h (cf. Fig. 3). Again the variation in E^{X} leads to the slight increase in τ, as displayed in Fig. 6 (b) for the nonpolar dot. For the polar dots, τ increases exponentially with increasing height h, stemming from the fact that f decreases dramatically with increasing dot height h (cf. Fig. 3). This results from both the increase in the built-in potential and the accompanied shift in E^{X} to lower energies, and thus contributing to the increase in τ.

Overall our theoretical calculations show that the radiative recombination lifetimes in c-plane systems strongly depend on the nanostructure size. However, this is not the case, at least when compared to the c-plane systems, for nonpolar InGaN/GaN dots. In the next section we will summarize the theoretical results and compare them to the experimental data obtained here and literature values.

6 Theory experiment comparison As discussed in the previous section, for the here chosen geometries and indium content of 15% we find τ values in the range of 435 ps to 500 ps. So far we have presented our theoretical data for τ as a function of the dot height or diameter. To compare theory with experiment more easily, we have re-plotted the theoretical data shown in Fig. 6 (b) for τ as a function of the exciton recombination energy E^{X}. The re-plotted data is displayed in Fig. 7. Comparing these results with the experimental values given in Fig. 2, several features are of interest. Firstly, we observe that for the here assumed geometry and indium content, the τ values obtained from theory are similar in magnitude to the experimental ones, but slightly higher. It should also be noted that the exciton recombination energies are larger than the experimentally measured QD emission energies. Thus with increasing the indium content above 15%, the excitonic transition energies would be shifted to values closer to the experimentally observed values. However, in doing so, since τ is inversely proportional to E^{X} as discussed before, τ should increase further, resulting in a larger disagreement between theory and experiment on τ. Conversely, when reducing the indium content below 15%, the agreement in τ between theory and experiment is improved, but the theoretical exciton recombination energies would be shifted to higher values. Therefore, further theoretical and experimental studies are required to extend this analysis. For instance, experimental insight into the indium content and the QD geometry is of

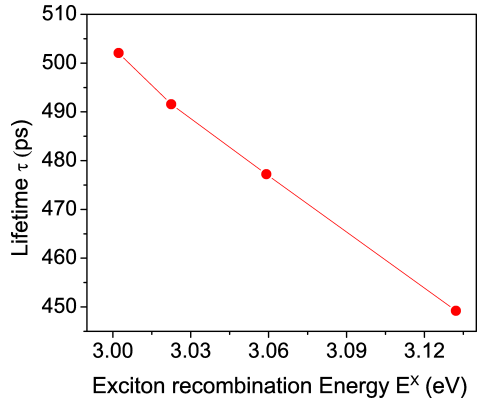

Figure 7 Recombination lifetime τ as a function of exciton recombination energy E^{X}.

central importance, since it gives input for the theoretical model. From a theoretical perspective, as discussed already in Sec. 3, uncertainties in the material parameters and their alloy dependence affect the calculated values. Moreover, as shown in nonpolar InGaN/GaN QWs [48], random alloy fluctuations lead to strong carrier localization effects which also affect radiative lifetimes. These alloy fluctuations inside a nonpolar InGaN/GaN QD could therefore also be important for a detailed understanding of the electronic and optical properties of a-plane QDs.

However, whilst the dots analysed for this paper present shorter lifetimes than those predicted by theory, our former analysis of other, similar structures, suggests somewhat longer lifetimes [19,47]. Values between 500-600 ps have for example been quoted in Refs. [19] and [47], which are in good agreement with the here presented theoretical data. Furthermore, the trend observed in the calculations that with decreasing E^{X} the radiative lifetime τ increases (cf. Fig. 7), is also vaguely visible in the experimental data (cf. Fig. 2). However, it should be noted that in the experiment the variations in lifetimes might also be affected by a combination of variations in indium content and dot size. Furthermore, in-plane shape asymmetries in a-plane QDs can also give rise to a spread in exciton energies due to changes in the QD volume and connected modifications in the built-in potential. The in-plane anisotropies have not been considered in the theoretical modeling. Nevertheless, the theoretical description presented gives radiative lifetimes which are comparable in magnitude to the experimental data obtained here and in previous studies, and forms now a good starting point for future combined experimental and theoretical investigations.

7 Summary and Conclusion In summary, we have presented a combined theoretical and experimental study of the radiative recombination lifetimes in a-plane $(11\bar{2}0)$ InGaN/GaN QDs. The structures have been grown by MDE and have been characterized by TRPL measurements. On the theoretical side a multiband $\mathbf{k}\cdot\mathbf{p}$ approach, coupled with self-consistent Hartree theory to account for excitonic effects, has been applied to gain insight into the optical properties of a-plane $(11\bar{2}0)$ InGaN/GaN QDs.

Our calculations show that for an accurate description of the optical properties of the here studied nonpolar InGaN QD systems Coulomb effects play a central role. For instance, we find here that the oscillator strength in a nonpolar system is almost unaffected by changes in the QD size, which is in contrast to its c-plane counterpart. While in the c-plane system the wavefunction overlap is dominated by the electrostatic built-in field, in the nonpolar case the attractive Coulomb interaction compensates the spatial separation of the charge carriers due to the residual built-in field. This leads to the situation that the radiative lifetime in the nonpolar system is one order of magnitude smaller when compared to the c-plane system. The calculated radiative lifetimes are in good agreement with literature data and comparable in magnitude to the here measured ones.

Overall our results indicate that nonpolar QDs are promising candidates for next generation visible wavelength single-photon emitters where the repetition rate compared to c-plane systems can be improved dramatically.

Acknowledgements This work was supported by Science Foundation Ireland (project number 13/SIRG/2210) and Engineering and Physical Sciences Research Council (EPSRC) UK (Grants EP/M012379/1 and EP/M011682/1).

References

[1] M. Gschrey, A. Thoma, P. Schnauber, M. Seifried, R. Schmidt, B. Wohlfeil, L. Krger, J. -H. Schulze, T. Heindel, S. Burger, F. Schmidt, A. Strittmatter, S. Rodt and S. Reitzenstein, Nat. Commun. **6**, 7662–8 (2015)
[2] X. Ding, Y. He, Z.-C. Duan, N. Gregersen, M.-C. Chen, S. Unsleber, S. Maier, C. Schneider, M. Kamp, S. Höfling, C.-Y. Lu and J.-W. Pan, Phys. Rev. Lett. **116**, 020401–6 (2016)
[3] R. Hafenbrak, S. M. Ulrich, P. Michler, L. Wang, A. Rastelli and O. G. Schmidt, New Journal of Physics **9**, 315–10 (2007)
[4] S. Deshpande, T. Frost, A. Hazari and P. Bhattacharya, Appl. Phys. Lett. **105**, 141109–5 (2014)
[5] M. J. Holmes, S. Kako, K. Choi, M. Arita, and Y. Arakawa, ACS photonics **3**, 543-546 (2016)
[6] E. Monroy, E. Munoz, F.J. Sanchez, F. Calle, E. Calleja, B. Beaumont, P. Gibart, J. A. Munoz and F. Cusso, Semicond. Sci. Technol. **13**, 1042-1046 (1998)
[7] E. Chernysheva, Z. Gacevic, N. G.-Lepetit, H. P. Van-der Meulen, M. Müller, F. Bertram, P. Veit, A. T.-Pardo, J.M.Gonzalez Calbet, J.Christen, E. Calleja, J.M.Calleja and S. Lazic, EPL **111**, 24001–6 (2015)
[8] A. F. Jarjour, R. A. Taylor, R. A. Oliver, M. J. Kappers, C. J. Humphreys and A. Tahraoui, Appl. Phys. Lett. **91**, 52101–3 (2007)
[9] H. Masui, J. Sonoda, N. Pfaff, I. Koslow, S. Nakamura and S. P DenBaars, J. Phys. D: Appl. Phys. **41**, 165105–6 (2008)
[10] M. A. Caro, S. Schulz, S. B. Healy and E. P. O'Reilly, J. Appl. Phys. **109**, 084110–10 (2011)

[11] A. D. Andreev and E. P. O'Reilly, Appl. Phys. Lett. **79**, 521-523 (2001)
[12] N. Baer, S. Schulz, S. Schumacher, P. Gartner, G. Czycholl, and F. Jahnke, Appl. Phys. Lett. **87**, 231114 (2005)
[13] P. Waltereit, O. Brandt, A. Trampert, H. T. Grahn, J. Menniger, M. Ramsteiner, M. Reiche and K. H. Ploog, Nature **406**, 865-868 (2000)
[14] U. T. Schwarz and M. Kneissl, Phys. Status Solidi. RRL **1**, A44-A46 (2007)
[15] S. Schulz and E.P. O'Reilly, Phys. Status Solidi. C **7**, 1900-1902 (2010)
[16] J. W. Robinson, J. H. Rice, A. Jarjour, J. D. Smith, R. A. Taylor, R. A. Oliver, G. Andrew, D. Briggs, M. J. Kappers, C. J. Humphreys and Y. Arakawa, Appl. Phys. Lett. **83**, 2674-2676 (2003)
[17] A. F. Jarjour, R. A. Oliver, A. Tahraoui, M. J. Kappers, C. J. Humphreys, and R. A. Taylor, Phys. Rev. Lett. **99**, 197403–4 (2007)
[18] R. A. Oliver, G. Andrew, D. Briggs, M. J. Kappers, C. J. Humphreys, S. Yasin, J. H. Rice, J. D Smith and R. A. Taylor, Appl. Phys. Lett. **83**, 755-757 (2003)
[19] T. Zhu, F. Oehler, B. P. L. Reid, R. M. Emery, R. A. Taylor, M. J. Kappers and R. A. Oliver, Appl. Phys. Lett. **102**, 251905–4 (2013)
[20] C. Johnston, M. Kappers, M. Moram, J. Hollander, and C. Humphreys, J. Cryst. Growth **311**, 3295-3299 (2009)
[21] M. Haberlen, T. J. Badcock, M. A. Moram, J. L. Hollander, M. J. Kappers, P. Dawson, C. J. Humphreys, and R. A. Oliver, J. Appl. Phys. **108**, 033523–7 (2010)
[22] A. F. Jarjour, A. M. Green, T. J. Parker, R. A. Taylor,R. A. Oliver,G. Andrew, D. Briggs, M. J. Kappers, C. J. Humphreys, R. W. Martin, I. M. Watson, Physica E **32**, 119-122 (2006).
[23] V. A. Fonoberov and A. A. Baladin, J. Appl. Phys. **94**, 11, 7178-7186(2003)
[24] N. Antoine-Vincent, F. Natali, M. Mihailovic, A. Vasson, J. Leymarie, P. Disseix, D. Byrne, F. Semond, and J. Massies, J. Appl. Phys. **93**(9), 5222-5226 (2003)
[25] M. Winkelnkemper, M. Dworzak, T. P. Bartel, A. Strittmatter, A. Hoffmann, and D. Bimberg, Phys. Status Solidi (b) **245**, 12, 2766-2770 (2008)
[26] O. Marquardt, S. Boeck, C. Freysoldt, T. Hickel , S. Schulz, J. Neugebauer and E. P. O' Reilly, Comput. Mater. Sci. **95**, 280-287 (2014)
[27] S. Boeck, C. Freysoldt, A. Dick, L. Ismer and J. Neugebauer, Computer Phys. Commun. **182**, 543-554 (2011)
[28] S. K. Patra, O. Marquardt and S. Schulz, Opt. Quant. Electron. **48**, 151–10 (2016)
[29] U. M. E. Christmas, A. D. Andreev, D. A. Faux, J. Appl. Phys. **98**, 073522–12 (2005)
[30] P. Rinke, M. Winkelnkemper, A. Qteish, D. Bimberg, J. Neugebauer and M. Scheffler, Phys. Rev. B. **77**, 075202–15 (2008)
[31] P. G. Moses, M. Miao, Q. Yan and C. G. Van de Walle, J. Chem. Phys **134**, 084703–11 (2011)
[32] S. Schulz and O. Marquardt, Phys. Rev. Applied **3**, 064020–17 (2015)
[33] H. H. Huang and Y. R. Wu, J. Appl. Phys. **107**, 053112–7 (2010)
[34] I. Vurgaftman and J. R. Meyer, J. Appl. Phys. **94**, 3675-3696 (2003)
[35] M. A. Caro, S. Schulz, and E. P. O' Reilly, Phys. Rev. B **86**, 014117–4 (2012)
[36] M. A. Caro, S. Schulz, and E. P. O Reilly, Phys. Rev. B **88**, 214103–22 (2013)
[37] J. Wu, J. Appl. Phys. **106**, 011101–28 (2009)
[38] Q. Yan, P. Rinke, M. Winkelnkemper, A. Qteish, D. Bimberg, M. Scheffler, and C. G. Van de Walle, Semicond. Sci. Technol. **26**, 014037–8 (2011)
[39] O. Stier, M. Grundmann and D. Bimberg, Phy. Rev. B **59**, 5688-5701 (1999)
[40] D. P. Williams, A. D. Andreev, E. P. O'Reilly, Superlattices Microstruct. **36**, 791-798 (2004)
[41] S. Shokhovets, G. Gobsch, and O. Ambacher, Appl. Phys. Lett. **86**, 161908 (2005)
[42] F. Ferdos, S. Wang, Y. Wei and A. Larsson, Appl. Phys. Lett. **81**, 1195-1197 (2002)
[43] S. Founta, F. Rol, E. Bellet-Amalric, J. Bleuse, B. Daudin, B. Gayral and H. Mariette, Appl. Phys. Lett. **86**, 171901–3 (2005)
[44] K. Schuh, S. Barthel, O. Marquardt, T. Hickel, J. Neugebauer, G. Czycholl and F. Jahnke, Appl. Phys. Lett. **100**, 092103–4 (2012)
[45] S. Barthel, K. Schuh, O. Marquardt, T. Hickel, J. Neugebauer, F. Jahnke and G. Czycholl, Eur. Phys. J. B **86**, 449–11 (2013)
[46] S. C. Davies, D. J. Mowbray, F. Ranalli and T. Wang, Appl. Phys. Lett. **96**, 251904–3 (2010)
[47] J. T. Griffiths, T. Zhu, F. Oehler, R. M. Emery, W. Y. Fu, B. P. L. Reid, R. A. Taylor, M. J. Kappers, C. J. Humphreys, and R. A. Oliver, APL Materials **2**, 126101–5 (2014).
[48] S. Schulz, D. P. Tanner, E. P. O'Reilly, M. A. Caro, T. L. Martin, P. A. J. Bagot, M. P. Moody, F. Tang, J. T. Griffiths, F. Oehler, M. J. Kappers, R. A. Oliver, C. J. Humphreys, D. Sutherland, M. J. Davies, and P. Dawson, Phys. Rev. B **92**, 235419 (2015)